Published in final edited form as:
J Cardiovasc Transl Res. 2011 October ; 4(5): 631–643. doi:10.1007/s12265-011-9292-0.

N-acetylglucosamine conjugated to nanoparticles enhances myocyte uptake and improves delivery of a small molecule p38 inhibitor for post-infarct healing

Warren D. Gray[1,2], **Paolin Che**[1,2], **Milton Brown**[1,2], **Xinghai Ning**[1], **Niren Murthy**[1,3,*], and **Michael E. Davis**[1,2,3,*]

[1]Wallace H. Coulter Department of Biomedical Engineering, Emory University and Georgia Institute of Technology, Atlanta, GA, USA

[2]Division of Cardiology, Emory University School of Medicine, Atlanta, GA, USA

[3]Parker H. Petit Institute for Bioengineering and Bioscience, Atlanta, GA

Abstract

An estimated 985,000 new myocardial infarctions (MI) will occur in the U.S. in 2011. While many will survive the initial insult, the early damage will eventually lead to heart failure for which the only definitive cure is transplantation. CM (CM) apoptosis is a large contributor to cardiac dysfunction, and although potential therapeutic molecules exist to inhibit apoptotic pathways, drug delivery methods are lacking. This damage is largely regional and thus localized delivery of therapeutics holds great potential; however CMs are relatively non-phagocytic, which limits existing options that rely on phagocytosis. Recently, the sugar N-acetyl-glucosamine (GlcNAc) was shown to be bound and internalized by CMs, providing a potential mechanism for drug delivery. Here we demonstrate efficacy of a drug delivery system comprising a drug-loaded biodegradable polyketal nanoparticle that is surface-decorated with GlcNAc. Inclusion of the sugar enhanced uptake by CMs as measured by intracellular activated fluorescence. When delivered *in vivo* following ischemia-reperfusion injury, GlcNAc-decorated particles loaded with the p38 inhibitor SB239063 reduced apoptotic events and infarct size, and improved acute cardiac function. This was in contrast to our published data demonstrating no acute effect of non-sugar decorated, p38 inhibitor-loaded particles. These data suggest a novel therapeutic option to enhance uptake of drug-loaded nanoparticles to CMs, and perhaps reduce the large amount of CM cell death following myocardial injury.

Keywords

myocardial infarction; nanoparticle; p38; polyketal

[*]Joint corresponding authors: Michael E. Davis, Ph.D, Assistant Professor of Biomedical Engineering and Medicine, The Wallace H. Coulter Department of Biomedical Engineering, Emory University and Georgia Institute of Technology, 101 Woodruff Circle, Suite 2001, Atlanta, GA 30322, USA, michael.davis@bme.emory.edu, Telephone: (404) 727-9858, Fax: (404) 727-9873. Niren Murthy, Ph.D., Associate Professor of Biomedical Engineering, The Wallace H. Coulter Department of Biomedical Engineering, Emory University and Georgia Institute of Technology, 315 Ferst Drive, Room 3303, Atlanta, GA 30332-0535, niren.murthy@bme.gatech.edu, Telephone: (404) 385-5145.

Conflict of interest statement

Drs. Davis and Murthy, as well as Emory University, are entitled to equity and royalties derived from Ketal Biomedical Incorporated, which is developing products related to the technology described in this paper. This study could affect his/her/their personal financial status. The terms of this arrangement have been reviewed and approved by Emory University in accordance with its conflict of interest policies.

Introduction

Myocardial infarction affects 985,000 new patients in the U.S. annually and is the leading cause of global morbidity and mortality [1]. During ischemic injury and in subsequent reperfusion [2], apoptotic signaling cascades in CMs are triggered, leading to localized death at the cellular level [3]. As adult CMs are terminally differentiated [4,5] and relatively non-proliferative [6], the ischemic insult leads to eventual dysfunction and failure at the organ level [7,8]. Because the initial cell death is primarily regional [9], localized therapy to target and reverse the damage to the injured myocardium is quite promising. Therefore, CM-specific rescue presents itself as a compelling therapeutic target following myocardial infarction.

Apoptotic pathways are complex and include many molecules, including whose activation either promote or inhibit cell death. Several proteins in these pathways have demonstrated a cardioprotective role, such as Bcl-2 [10,11], Bcl-xL [12], and XIAP [13]. Other proteins outside of apoptotic pathways also improve cell survival, such as SOD and Catalase that attenuate oxidative stress produced during ischemia-reperfusion (IR) injury [14,15]. Furthermore, expression and activity of these proteins are regulated by intracellular signaling molecules such as c-jun N-terminal kinase (JNK) [16,17], AKT [18], and p38 [19] to name a few. Whereas many of these kinases have specific small molecule inhibitors, delivery and toxicity concerns due to the need for large systemic doses preclude their use.

While overexpressing anti-apoptotic proteins and antioxidants in CMs has shown functional improvements in animal models [20–24], many delivery hurdles prevent clinical translation. The short circulation half-life of these proteins and small molecules [25] precludes systemic delivery due to the need for extended exposure to large amounts of therapeutic needed. To address this concern, many studies have been performed using biomaterials for sustained, local delivery [26–30]. Despite some successes, methods to deliver drugs to the infarct currently rely on passive release into the interstitium from delivery vehicles or internalization by phagocytic cells. As the majority of phagocyctic cells accumulate 24–72h following IR injury [31], delivery vehicles that rely on passive macrophage-mediated release do not inhibit the excessive apoptosis that occurs in CMs during the initial 72h. Drug delivery vehicles that target CMs are virtually nonexistent, owing largely to the non-phagocytic nature of these cells. However, recent studies have implicated *N*-acetyl-D-glucosamine (GlcNAc) as a viable candidate for a drug delivery system targeted to CMs, demonstrating the ability of CMs to bind to and internalize GlcNAc-decorated liposomes [32,33]. The use of liposomes as a drug delivery vehicle, however, may lead to challenges: leakage of water-soluble drugs during preparation and storage is a known disadvantage; and the destabilization of liposomes in the presence of high-density lipoproteins in blood plasma limits its use [34].

Previously, we inhibited chronic cardiac dysfunction through the controlled release of the p38 inhibitor SB239063 from microparticles into the extracellular region of the post-infarcted heart [30]. Despite this improvement in chronic function, there was no change seen in early function, indicating release was not fast enough or the inhibitor was not taken up by the appropriate cell type. *In vitro*, macrophages readily phagocytosed the particles whereas other cell types did not, most likely due to lack of targeting agents. In this study, we developed a drug delivery system for enhanced CM uptake by decorating degradable, biocompatible polymeric nanoparticles (polyketals) with GlcNAc (cartoon depiction in Figure 1) and demonstrated its ability to be internalized by CMs. Using these GlcNAc particles, we were able to reduce infarct size and improve acute cardiac function in strong contrast to our published data with unmodified polyketals.

Materials and Methods

Synthesis of GlcNAc-alkyl

GlcNAc-alkyl (**1**) was synthesized by clicking an azide-modified GlcNAc (**6**) onto an alkyne-functionalized alkyl-hexaethylene glycol (**7**) (shown in Figure 2). The azide-modified GlcNAc (**6**) was synthesized by functionalizing the anomeric carbon of GlcNAc (**2**) in three steps. Briefly, the hydroxyl groups of GlcNAc were protected with acetic anhydride in pyridine, generating (**3**). The anomeric acetyl of (**3**) was activated with lewis acid to form the oxazoline donor, and then coupled with azido-propanol, using TMSOTf as the catalyst to afford the desired derivative (**6**). The final product GlcNAc-alkyl (**1**) was synthesized by clicking the GlcNAc (**6**) onto the alkyl-hexaethylene glycol (**7**) in presence of catalyst copper(I) bromide, followed by deacetylation. The identities of final and intermediate species were confirmed by ^{1}H- and ^{13}C-NMR and mass spectrometry. Compound (**1**) ^{1}H NMR (400 MHz, CDCl3): δ (ppm) 7.57 (s, 1H, triazole), 4.94 (t, 1H, J = 8.8 Hz), 4.56 (m, 2H), 4.48 (m, 1H), 4.36–4.33 (m, 2H), 4.14–4.12 (m, 2H), 3.77–3.57 (m, 26H), 3.25 (m, 2H), 3.30 (m, 2H), 2.07 (m, 2H), 1.98 (s, 3H), 1.40 (m, 2H), 1.22–1.13 (m, 31H). ^{13}C NMR (100 MHz, CDCl3): δ (ppm) 173.8, 156.4, 145.1, 123.5, 101.2, 76.7, 75.7, 70.7, 70.5, 70.4, 70.3, 69.7, 65.2, 64.5, 63.6, 61.6, 56.6, 53.4, 46.6, 41.0, 31.9, 30.1, 29.9, 29.7, 29.6, 29.5, 29.3, 29.2, 26.7, 23.3, 22.7, 14.1. HRMS (FAB): m/z calculated for $C_{43}H_{81}N_5O_{14}$ $[M+Na]^+$: 914.6, found: 914.6.

PCADK synthesis

PCADK was synthesized as previously described [28]. Briefly, 2,2-dimethoxypropane was reacted with 1,4-cyclohexanedimethanol in an acetal exchange reaction in distilled benzene at 100°C with p-toluenesulphonic acid as the polymerization catalyst. 2,2-dimethoxypropane was supplied to the reaction in an equimolar ratio to 1,4-cyclohexanedimethanol. To compensate for the loss of benzene and 2,2-dimethoxypropane through distillation, additional amounts were added every two hours. At 8h, a small amount of triethylamine was added to the reaction vessel to stop the reaction. Adding this reaction mixture dropwise to cold hexanes (−20°C) precipitated out the polymer, which was then removed by vacuum filtration and dried prior to particle formation.

Particle production

Polyketal particles loaded with rhodamine B (Sigma-Aldrich) (PK-GlcNAc-rhodamine) were prepared via a solvent displacement method. Briefly, a solution of 40 mg poly(cyclohexane-1,4-diyl acetone dimethylene ketal) (PCADK) and 0.2 mg Rhodamine B in 8 mL tetrahydrofuran was added dropwise into a vigorously stirred aqueous solution of 1% GlcNAc-alkyl. The resulting stirred suspension was vented for 6h to allow for evaporation of solvent.

Polyketal particles loaded with 5-chloromethylfluorescein diacetate (Invitrogen) (PK-GlcNAc-CMFDA), (9′-(4-(and 5)-chloromethyl-2-carboxyphenyl)-7′-chloro-6′-oxo-1,2,2,4-tetramethyl-1,2-dihydropyrido[2′,3′-6]xanthene (Invitrogen) (PK-GlcNAc-CMRA), or SB239063 (Axxora) (PK-GlcNAC-SB) were generated using an emulsion-solvent evaporation technique. Fifty mg of PCADK and cargo (0.25 mg CMFDA, 100 μg CMRA, or 0.5 mg SB239063) were dissolved in 1 mL of dichloromethane. The polymer solution was then added to 7 mL of 5% polyvinyl alcohol (PVA) and 5 mg GlcNAc-alkyl (or 0.5 mg GlcNAc-alkyl for 1% decoration of PK-GlcNAc-CMFDA particles), homogenized at high speed for 60s, and sonicated for 30s to produce nanoparticles. The resulting emulsion was transferred to 30 mL of 0.5% PVA and stirred at approximately 100 rpm for 4h to allow for evaporation of solvent. All of the particle suspensions were then centrifuged and washed with deionized water three times to remove residual PVA and GlcNAc-alkyl, as well as non-

encapsulated cargo. The suspension was then snap frozen in liquid nitrogen and lyophilized to produce a free flowing powder.

Particle characterization

Particles were sized by a Wyatt DynaPro Nanostar dynamic light scattering (DLS) instrument (Wyatt Technology) and imaged by a Zeiss Ultra 60 scanning electron microscope (SEM). Nanoparticle circumferences were traced using ImageJ software to confirm DLS-determined sizes. Zeta potentials of particles in PBS buffer (pH 7.4) were measured by a Malvern Instruments Zetasizer.

To determine cargo content, loaded and non-loaded particles were hydrolyzed overnight in 1 N HCl. Quadruplicates of 1 mg each of CMFDA-loaded nanoparticles (0%, 1%, and 10% decorated PK-GlcNAc-CMFDA particles) were hydrolyzed in 100 μL HCl at 80°C for 3h. To activate CMFDA fluorescence, 200 μL $Ba(OH)_2$ was added to each sample heated at 80°C for 3h. Following neutralization with 10x PBS, solutions were snap frozen in liquid N_2 and and lyophilized to concentrate CMFDA. All readingsz were performed in 100 μL PBS, and fluorescence determined via plate reader (exc/emi = 492/517 nm) (BioTek Synergy 2) and loading amount calculated from a standard curve generated using free CMFDA (r^2=0.99). The absorbance of resultant solutions containing SB239063 was measured at 320 nm and loading efficiencies calculated from a standard curve generated using free SB239063 (r^2=0.99).

Degree of decoration was measured by first hydrolyzing 5 mg of PK-GlcNAc (with a theoretical decoration of 10% and 1%) and PK particles (in triplicate) in 1 N HCl, followed by neutralization with NaOH. The absorbance of the resulting solutions was measured at 278 nm in a plate reader and wt% decoration calculated from a standard curve generated from free GlcNAc-alkyl (r^2=0.99). GlcNac-alkyl decoration was orthogonally confirmed by analyzing molecular species by electrospray ionization mass spectrometry.

SB release characterization

2 mg of PK-GlcNAc-SB and PK-GlcNAc particles in triplicate were suspended 1 mL PBS (pH 7.4) and set on an inverting rotator (0.25 Hz) at 37°C. At specified timepoints, suspensions were spun at 13.3 rpm for 5 min to pellet particles and 100 μL supernatant removed for analysis. 100 μL fresh PBS was added to compensate and particles resuspended. The absorbance of the samples was measured at 320 nm and concentration calculated from a standard curve of free SB239063 (r^2=0.99). At the end of the experiment, the particles were hydrolyzed to determine the amount of remaining SB, and a release curve was generated accounting for amount of SB released from and remaining in particles.

CM isolation

CMs were isolated from day-old Sprague Dawley rat pups as previously described [32,29]. Briefly, excised rat hearts were washed with Hank's Balanced Salt Solution and minced, followed by extracellular matrix digestion in 1 mg/mL trypsin solution in a rotating shaker at 4°C for 6h. Following centrifugation, the supernatant was removed and pellet re-suspended in 0.8 mg/mL collagenase solution. The suspension was incubated at 37°C for 10 min and filtered through 70 μm syringe filter. To remove vascular smooth muscle cells and endothelial cells, the suspension was plated for 1h in fibronectin-coated T75 flasks. The non-adherent cells were removed and plated in fibronectin-coated 6- or 12-well plates in antibiotic-supplemented DMEM media (10% FBS). Twelve hours before treatment, cells were quiesced in serum-free media.

Imaging of rhodamine-loaded particles in cells

A 0.5 mg/ml particle suspension of rhodamine-loaded, GlcNAc-decorated particles in serum-free DMEM media was added to quiesced CMs. After incubation at 37°C for 12h, cells were washed three times with phosphate buffered solution and cells fixed in 4% paraformaldehyde. Following membrane permeabilization, immunostaining was performed with mouse anti-α-actinin (Sigma-Aldrich) and DAPI to stain nuclei. Cells were imaged with a Zeiss 510 META confocal laser scanning microscope.

Determining uptake of CMFDA-loaded particles in cells

A 0.5 mg/ml suspension of CMFDA-loaded or non-loaded particles with varied levels of GlcNAc decoration was prepared in serum-free DMEM media and added to quiesced CMs. Following incubation at 37°C for 12h, fluorescence of cells was measured by plate reader (exc/emi = 492/517 nm).

Treatment of CMs with PK-GlcNAc-SB

Quiesced cells were incubated with 0.5 mg/mL of PK-GlcNAc-SB or PK-GlcNAc particles in serum-free DMEM at 37°C for 18h, followed by stimulation with TNF-α (10 μg/mL) 20 min. Cells were harvested in lysis buffer with protease and phosphatase inhibitors. Western analysis for p38 activation was performed on 35 μg of protein lysate. Following SDS-PAGE separation, proteins were transferred to a nitrocellulose membrane and probed with antibodies against phosphorylated or total p38 (Cell Signaling).

Animal studies

Randomized and blinded studies were conducted using adult male Sprague-Dawley rats (obtained from Charles River) weighing 250 g. Rats were subjected to ischemia-reperfusion (IR) injury as described previously [35]. Briefly, under isoflurane anesthesia (1–3%), the left anterior descending coronary artery was occluded for 30 minutes using an 8-0 prolene suture. Following occlusion, reperfusion was initiated by removal of the suture and animals were divided into treatment groups. Particle suspension treatments were given in 100 μL of sterile saline into the perimeter of cyanotic ischemic zone (3 locations) through a 30-gauge needle immediately after reperfusion. The survival rate of animals during surgery was 80%, and 100% during recovery. All animal studies were approved by Emory University Institutional Animal Care and Use Committee.

To examine *in vivo* uptake of particles, rats were divided into three treatment groups: saline alone, PK-CMRA, and PK-GlcNAc-CMRA (*n*=3 for each group). Three days following IR and treatment, rats were sacrificed and hearts excised. After preservation in Optimal Cutting Temperature (OCT) compound (Tissue-Tek), hearts were sectioned into 7 μm thick slices and immunostaining performed with anti-α-actinin (Sigma-Aldrich) and DAPI to stain nuclei. Tissues were imaged with a Zeiss 510 META confocal laser scanning microscope (CMRA exc/emi = 548/576 nm).

In vivo reduction of apoptotic events was explored by dividing the rats into three treatment groups: saline alone, empty PK-GlcNAc, and PK-GlcNAc-SB (*n*=3 for each group). One day following IR and treatment, rats were sacrificed and hearts excised. After cryopreservation in OCT compound, hearts were sectioned and subject to immunostaining for α-actinin and DAPI. Tissues were subject to TUNEL *in situ* apoptosis detection, TMR red (Roche) to stain for apoptotic nuclei and imaged with a Zeiss Axioskop microscope. Using Image-Pro Plus software (MediaCybernetics), apoptotic and total nuclei were tallied and extent of apoptosis calculated for each treatment group.

For structural and functional experiments, rats were split into three groups: saline alone, PK-GlcNAc, and PK-GlcNAc-SB (n>7 for each group, N=29 total). Additionally, some animals received sham surgery. Echocardiography was performed three days following surgery. The animals were sacrificed and immediately perfused for infarct size measurements.

Echocardiography

Rats were anesthetized with inhaled isoflurane (1–3%; Piramal) and subjected to echocardiography 3 days after IR surgery. Short axis values of left ventricular end systolic (ES) and end diastolic (ED) dimension were obtained using a Vevo® 770 echocardiography workstation with a high frequency transducer. An average of 3 consecutive cardiac cycles was used for each measurement and was made 3 times in an investigator-blinded manner.

Infarct size

Three days following IR, animals were sacrificed and isolated hearts perfused at 37°C retrograde through the aorta with Krebs-Hepes buffer. The coronary artery was then re-occluded with the suture that was left in place at the time of reperfusion and the heart was perfused with filtered Evan's blue dye to define the left ventricle (LV) area at risk. The LV was sliced into cross-sections followed by 2 min soaking in 1% 2,3,5-triphenyltetrazolium chloride (TTC) solution at 37°C to stain viable myocardium, followed by fixing in 4% paraformaldehyde. Each section was photographed for analysis. Noninfarcted tissue (region outside the ligated area) was identified by deep blue staining, ischemic but viable myocardium was identified by deep red staining (at-risk area), and non-viable LV tissue was identified by white coloration. ImageJ software was used to trace the three areas in all sections. The areas of the three regions from all slices were summed for each heart and data were expressed as infarct size/area-at-risk.

Statistics

All statistics were performed using GraphPad Prism software.

Results

CM internalization of PK-GlcNAc-rhodamine nanoparticles

Cultured CMs harvested from day-old Sprague-Dawley rat pups were incubated with rhodamine-loaded, GlcNAc-decorated particles prepared by a solvent displacement method. Particles were imaged by SEM and analyzed by ImageJ software and had an average diameter of 320±156 nm (mean±SD; Figure 3a). Cells were incubated with particles for 6h and analyzed by confocal microscopy to visualize particle uptake. To determine cell morphology, sections were counterstained with the cardiac-specific marker α-actinin (green) and images were merged to determine overlay. As demonstrated in the orthogonal images, rhodamine-loaded GlcNAc particles (red) were internalized by CMs (Figure 3b).

CM internalization of PK-GlcNAc-CMFDA nanoparticles in vitro

To further demonstrate particle internalization, GlcNAc-decorated (0%, 0.6%, 9% as determined experimentally) CMFDA-loaded nanoparticles were prepared via a single emulsion method. Following hydrolysis of particle samples and fluorescence activation, average CMFDA encapsulations were determined by plate reader to be 2.9, 5.1, and 4.3 nmol CMFDA/mg particle for 0%, 0.6%, and 9% sugar decoration, respectively (Figure 4a).

The fluorescence of cultured CMs treated with CMFDA-loaded nanoparticles for 12h was determined by plate reader and normalized to the 0% GlcNAc particles and the respective particle CMFDA content. Cells treated with 0.6% GlcNAc decorated particles exhibited a

1.4±0.1-fold increase in fluorescence, whereas treatment with 9% GlcNAc particles resulted in a significant 2.8±0.1-fold increase in fluorescence over cells treated with CMFDA-loaded, non-decorated particles (mean±SEM; n=4; *p<0.01, ***p<0.001. ANOVA; Figure 4b).

In vitro inhibition of p38 activation

PK-GlcNAc-SB and PK-GlcNAc particles were prepared by a single emulsion method and had a mean diameter of 370 nm by SEM image analysis and DLS (Figure 5a&b). A cumulative release curve of SB239063 from PK-GlcNAc-SB particles was generated, with 24% released by day 5 in a 2 mg/mL suspension (Figure 5c)

To evaluate *in vitro* particle internalization, CMs were pretreated with serum free media alone or particles for 18h and stimulated with TNF-α (10 μg/mL) for 20 minutes. Proteins were run on SDS-PAGE gel and membranes were stained for both phosphorylated and total p38 levels. Band densities were calculated by Carestream Health Imaging software. The amount of p38 phosphorylation (p-p38) was normalized to total p38 for each treatment (Figure 5d). TNF-α stimulation significantly increased p-p38 over basal levels in PK-GlcNAc pretreated CMs (0.7±0.1 to 1.8±0.2), but not in the PK-GlcNAc-SB pretreated cells. Additionally, the amount of TNF-α-stimulated p-p38 was significantly decreased in PK-GlcNAc-SB cells compared with PK-GlcNAc pretreatment (1.8±0.2 vs. 0.7±0.3; mean ±SEM; n=3; p<0.05; ANOVA followed by Tukey post-test).

In vivo uptake of PK-GlcNAc-CMRA particles and apoptotic inhibition by PK-GlcNAc-SB particles

To examine the ability of the GlcNac-decorated particles to be internalized *in vivo*, a blinded and randomized model of ischemia-reperfusion (IR) injury was used. Following 30 minutes of ischemia, the left ventricle was reperfused and rats received injections of saline, PK-CMRA (average diameter=443 nm), or PK-GlcNAc-CMRA (average diameter=453 nm) particles in a randomized and blinded manner (n=3 for each group). Three days following IR, animals were sacrificed and hearts excised, snap frozen in OCT compound, and sectioned. Using immunohistochemistry, CMs were identifiable by α-sarcomeric actinin staining (green). CMRA-positive cells were identified by red fluorescence, and representative co-localization images are shown in Figure 6a. Qualitative data from the images suggest efficient *in vivo* uptake of PK-GlcNAc-CMRA with little staining in PK-CMRA treated animals.

After establishing that GlcNAc-decorated particles are internalized by CMs *in vivo*, we sought to evaluate the anti-apoptotic effect of PK-GlcNAc-SB particles *in vivo* in a randomized and blinded manner. Using the IR rat model, we injected saline, PK-GlcNac, and PK-GlcNAc-SB particles (n=3 for each group) into the border zones of the left ventricle as described in the methods. Twenty-four hours following IR, the rats were sacrificed, and TUNEL staining was performed for identification of the apoptotic nuclei (purple color; Figure 6b) of α-sarcomeric actinin-positive cells (green). The number of apoptotic CMs for each treatment group was determined and expressed as a percent of total CMs counted. We found that delivery of PK-GlcNAc-SB particles to the heart significantly reduced the percentage of apoptotic myocytes in the infarcted area as identified by TUNEL staining (Figure 6b). In saline-only and PK-GlcNAc treated rats, 83%±14% and 64%±4% of CMs counted were TUNEL-positive (Figure 6c). However, a significantly lower number of apoptotic CMs were counted in hearts treated with PK-GlcNAc-SB particles (23%±6%) (**p<0.05 and *p<0.01; ANOVA followed by Newman-Keuls post-test). Taken together, these data suggest that GlcNAc decoration of particles enhanced CM uptake *in vivo*, and delivered anti-apoptotic signals following IR.

In vivo cardiac function

We next sought to determine the ability of the SB-loaded particles to rescue rats from acute cardiac dysfunction. Following 30 minutes of ischemia, the left ventricle was reperfused and rats received injections of saline, PK-GlcNAc, or PK-GlcNAc-SB particles in a randomized and blinded manner. Three days following IR, rats were subjected to small animal echocardiography (n=4 for sham, n>7), prior to determination of infarct size using TTC staining. Saline treated rats had an infarct size/area-at-risk (IS/AAR) of 43.7%±5.6% (Figure 6a). While no significant difference was seen in rats that received PK-GlcNAc particle injection post-IR (IS/AAR = 49.4%±3.1%), rats that received PK-GlcNAc-SB particles had a significant reduction in IS/AAR (28.4%±3.2%; p<0.05 vs. IR and p<0.01 vs. PK-GlcNAc; ANOVA).

To determine functional changes, left ventricular diameters were measured at peak systole and diastole to determine fractional area of shortening (n=5). Sham-operated rats had a fractional shortening (FS) of 50.5%±0.9% that was significantly lower in IR animals (39.6% ±0.7%; p<0.05; ANOVA) (Figure 6b). While no significant increase was seen in PK-GlcNAc treated rats (38.6%±1.7%), treatment with PK-GlcNAc-SB significantly improved FS (44.4%±1.2%; p<0.05 vs. IR, p<0.05 vs. PK-GlcNAc; ANOVA). Taken together, these data demonstrate a positive effect of PK-GlcNAc-SB on cardiac function following IR.

Discussion

Apoptosis of CMs following IR is suggested to be the dominant cause of chronic heart failure [7,8], but despite the existence of molecules with the potential to inhibit apoptotic pathways, development of vehicles for intracellular drug delivery into CMs remains a large challenge for post-MI healing. Systems exist for sustained extracellular release of therapeutic molecules or that act through phagocytic cells, such as macrophages. However, potential therapeutics that act intracellularly are precluded from existing systems due to their inability to transmigrate cell membranes. Previous studies discovered that CMs bind to and internalize GlcNAc, providing a compelling targeting agent in CM-targeting drug delivery systems [32]. The researchers delivered pravastatin (a 3-hydroxy-3-methylglutaryl-CoA reductase inhibitor)-loaded GlcNAc-decorated liposomes to CMs and following stimulation with interleukin-1β, showed enhanced nitric oxide production and inducible nitric oxide synthase expression. However, the studies were limited to *in vitro* experiments and relied on liposomal vehicles, which are known to be unstable and leak water-soluble contents [34]. In our approach, we decorated acid-sensitive nanoparticles with GlcNAc and validated our delivery system both *in vitro* and *in vivo. O*ur preliminary findings implicate GlcNAc-decorated nanoparticles as a novel method of delivering therapeutic molecules to CMs to heal the post-infarct heart.

In this report, we synthesized a targeting molecule consisting of GlcNAc tethered to an alkyl chain via a PEG linker. This was completed in a facile 8-step process with inexpensive materials. The reactions were conducted at the gram scale, but are scalable to kilogram quantities, allowing for larger production applications. Through hydrophobic interactions, the hydrophobic tail associated with the polymeric particle, allowing for the more hydrophilic sugar head group to partition into the aqueous phase to interact with CMs. In fact, this proposed particle-GlcNAc-alkyl interaction proved effective in decorating particles: in initial formulations of 10% and 1% by weight GlcNAc-alkyl to PCADK, the actual degree of decoration was 9 wt% and 0.6 wt%, respectively. This decoration of hydrophobic polymeric particles with hydrophilic GlcNAc increased the zeta potential from −8.97 mV (0% decoration) to −3.39 mV (9% decoration). We have used this strategy in prior studies to bind large proteins to the outside of microparticles. Additionally, this strategy is not all that uncommon and is used to surface modify hydrophobic polymers with

hydrophilic molecules [29,36]. The polymer was composed of the polyketal PCADK that degrades in acidic environments, such as in the developing endosome. The byproducts are biocompatible (acetone is on the GRAS list and 1,4-cyclohexanedimethanol is FDA approved as an indirect food additive and has an excellent animal toxicity profile [28]) and PCADK particles have been shown to neither incite the inflammatory response nor induce cell death [30]. We are able to routinely produce nanoparticles ranging in size from 200 to 800 nm, which is small enough to allow for cell internalization and large enough to avoid being flushed from the injured myocardium.

To initially demonstrate enhanced cellular uptake due to GlcNAc-decoration, particles were loaded with rhodamine B and incubated with CMs. Confocal images taken 12h later presented evidence of particle internalization wherein red nanoparticles were positioned within cells, visible within orthogonal frames. However, to more quantifiably determine internalization, we produced size- and load-matched particles with 0%, 1%, or 10% GlcNAc-alkyl decoration that contained the cell tracker dye CMFDA. The dye is non-fluorescent until activated by intracellular esterases and becomes cell impermeant by reaction with glutathione, thus fluorescence should only been seen when the CMFDA is released from the particles into the cell. To account for any CMFDA release from non-internalized particles, we normalized fluorescent readings to non-GlcNAc decorated CMFDA-loaded particle treatment. This approach allowed us to attribute fluorescence increase only with internalized particles. By comparing against the 0% decoration control, we saw a significant increase in fluorescence at 10% GlcNAc decoration, which confirmed that increasing GlcNAc decoration enhanced cellular uptake. While particle hydrolysis is possible outside the cell, which would allow release of the cell permeable CMFDA in the media, our published studies would argue against that. The hydrolysis half-life of PCADK polymer at pH 7.4 was four years in serum-free media [28], and thus it was unlikely that significant amounts of the hydrophobic CMFDA were released into the media. Furthermore, we examined release of CMFDA over 12h in cell free conditions and found no differences between the different particle preparations (data not shown). The positive trend between degree of GlcNAc decoration and fluorescence increase implicates varying GlcNAc decoration to tune internalization kinetics, though more data points are needed. Moreover, it was suggested in prior studies that oligosaccharide decoration may also enhance uptake, setting the stage for a multi-sugar decorated particle to alter cell specificity [33]. We did not explore the mechanism for GlcNAc internalization, but findings from a recent study indicate that the intermediate filaments vimentin and desmin possess lectin-like domains on the cell surface that bind to and internalize GlcNAc [33]. Although vimentin and desmin are not unique to CMs, they are enriched in muscle cells [37] and gene knockouts demonstrate negative cardiac phenotypes [38].

The mitogen activated protein kinase p38 is known to be a key regulator of apoptotic pathways and is triggered by IR [39–41]. While our prior studies confirmed that PCADK was able to deliver therapeutics to macrophages, significant activation of p38 in CMs leads to apoptosis, activation of inflammatory genes, and stimulation of pro-fibrotic factors. Previously, we incubated CMs with SB-loaded non-decorated PCADK particles and analyzed TNF-stimulated p38 activation at several time points. We found no significant decrease in activated p38 when comparing inhibitor loaded and empty PCADK particles up to 6h (unpublished data), indicating that CMs internalized little non-sugar decorated particle, correlating with our current study using CMFDA. As our CMFDA data demonstrated significant uptake at 18h, we used this time point to determine efficacy of our inhibitor-loaded GlcNAc particles. After 18h of incubation with PK-GlcNAc or PK-GlcNAc-SB, we examined kinase activity by measuring TNF-α-stimulated p38 phosphorylation. We found that while PK-GlcNAc (empty particle) treatment did not prevent p38 activation by TNF-α, treatment with PK-GlcNAc-SB did prevent this activation, suggesting internalization of

particles and release of the inhibitor. Additionally, p38 activation was verified through a no particle control treatment, with a 1.8-fold increase in p-p38 due to TNF-α treatment (data not shown). The delivery of SB239063 to cells via non-internalization means (i.e. extracellular release) in the acute phase is relatively low; our release curve indicates that only up to 13% of SB may be released outside cells at pH 7.4 within three days. Though the current study only examined a small molecule p38 inhibitor, we have demonstrated the ability of PCADK particles to encapsulate a broad range of compounds from siRNA to proteins, and future work will determine whether these cell impermeant factors can also be delivered intracellularly to CMs.

To evaluate the applicability of our GlcNAc-decorated nanoparticle as a drug delivery system to CMs *in vivo*, we first examined the enhanced uptake of GlcNAc-decorated particles and then the anti-apoptotic effect of PK-GlcNAc-SB particles before assessing functional responses. We injected a saline particle suspension into the myocardium immediately following IR and evaluated cardiac function and structure in the acute temporal window. Although injection of small molecule therapeutics would be possible in a clinical setting, small molecules are cleared quickly from the well-perfused heart. We examined direct particle injection to the myocardium as intramyocardial injections in humans has been performed for cell therapy applications and is considered safe [42–44]. Although signaling cascades persist for weeks following MI and therapeutic treatments would benefit from sustained delivery, acute therapies are also needed. Our published data demonstrated that sustained inhibition of p38 by particles *in vivo* had a chronic—but little acute—benefit. Therefore we hypothesized that delivery of particles with enhanced CM uptake would improve acute myocyte survival. We qualitatively found that more CMs internalized CMRA-loaded particles due to GlcNAc decoration, validating *in vivo* applicability of this delivery system. Furthermore, the anti-apoptotic effect of PK-GlcNAc-SB particles was successfully demonstrated *in vivo* following IR through the use of TUNEL staining: a 3.6-fold decrease in apoptotic CMs was observed due to PK-GlcNAc-SB treatment from the saline-only treatment. While the levels of TUNEL-positive cells in our studies seem rather high, it is important to note that much of our measurement comes from the border zones as that is where therapy was introduced. A more thorough study of apoptosis is underway.

In the structural response of rat model, no significant reduction in infarct size was seen between IR and PK-GlcNAc treatments, indicating no benefit of the empty sugar particle. However, delivering PK-GlcNAc-SB particles to the injured myocardium significantly decreased infarct by 35% from IR animals, indicating improved myocyte survival. While CM survival was not directly measured via cellular markers, infarct size is a well-known indicator of CM damage. This protective effect of PK-GlcNAc-SB was not only seen on infarct size, but cardiac function as well. Our data demonstrated significant decreases in fractional shortening in IR and PK-GlcNAc groups as compared with sham-operated animals. However, PK-GlcNAc-SB particle treatment restored nearly 50% of lost function over IR levels. While this was not restored to sham levels, the improvement was significant and indicates a functional benefit of GlcNAc-decorated particles loaded with a p38 inhibitor.

We did not directly compare with non-decorated, inhibitor-loaded particles in our current study because it was unnecessary to duplicate negative data we previously produced utilizing animal studies [30]. In that study, rats that received the p38-loaded inhibitor in PCADK particles had fractional shortening values similar to empty GlcNAc particle- and saline-treated IR rats (below 40%). Statistical comparison indicated no significant differences between those treatments, and PK-GlcNAc-SB was significantly improved over PCADK-SB particles, despite it being a separate study. It is important to note that we did not examine long-term function in this study, and the effect of sugar decoration on particle efficacy in the chronic phase is unknown. As our prior barrier was lack of efficacy during

the acute phase, we only examined this time point. One would hypothesize that increasing CM uptake would lead to a rapid depletion of drug-loaded nanoparticles available in the myocardium. While some studies suggest that inhibiting early apoptosis is critical for long-term function [45,46], our prior studies with encapsulated superoxide dismutase suggest that inhibition of apoptosis alone may not be sufficient for long-term improvements [35]. Thus, the optimal therapy may involve a mixture of decorated and non-decorated nanoparticles to target both phases of post-MI cardiac dysfunction. In future studies, we will determine the long-term benefit of PK-GlcNAc-SB treatment and determine whether this early rescue of function leads to long-term improvements; or if combination with PCADK-SB particles that chronically inhibited p38 in macrophages gives a synergistic effect. Finally, despite the fact that GlcNAc glycosylation of proteins improves function of CMs and may play a role in the response following infarction [47], we saw no beneficial effect of empty PK-GlcNAc particles. The studies demonstrating a critical role for this sugar did so by altering the activity or expression of the enzyme O-GlcNAc transferase (OGT). Thus the potential exists for the empty PK-GlcNAc particles to possess bioactivity in the setting of altered OGT activity. While not explored in this paper, encapsulation of OGT within PK-GlcNAc nanoparticles could have therapeutic potential.

Conclusion

In summary, our work demonstrates that GlcNAc-decorated nanoparticles can be effective vehicles for intracellular delivery of therapeutic molecules to CMs. As verified by confocal microscopy and fluorescent plate readouts, CMs effectively internalized dye-loaded GlcNAc-decorated particles. Additionally, we demonstrated *in vitro* therapeutic delivery of the p38 inhibitor, SB239063, to CMs and validated GlcNAc-decorated nanoparticles as *in vivo* delivery vehicles by decreasing infarct size and restoring cardiac function. The lack of uptake of some molecules by non-phagocytic CMs, toxic doses required of others, and sustained temporal availability preclude systemic delivery of most therapeutics as a method of treatment following MI. With the large scalability and non-toxic nature of the nanoparticles, as well as the ability to encapsulate a variety of compounds, the clinical potential is quite compelling. The proposed delivery system described in this study demonstrates a potential means to enrich intracellular therapeutics within CMs, providing a novel vehicle for treatment for acute myocardial function and possible prevention of heart failure resulting from massive CM death.

Acknowledgments

This work was supported by the National Heart, Lung, and Blood Institute, National Institutes of Health, as a Program of Excellence in Nanotechnology Award, N01 HV-08234, to NM and MED. Additionally, this work was supported by award HL090601 from the National Institutes of Health to MED, as well as a GAANN Fellowship from the Center for Drug Design, Development, and Delivery at Georgia Institute of Technology to WDG.

References cited

1. Lloyd-Jones D, Adams RJ, Brown TM, Carnethon M, Dai S, De Simone G, Ferguson TB, Ford E, Furie K, Gillespie C. Heart disease and stroke statistics--2010 update: a report from the American Heart Association. Circ. 2010; 121 (7):e46.
2. Maulik N, Yoshida T, Das DK. Oxidative stress developed during the reperfusion of ischemic myocardium induces apoptosis. Free Radic Biol Med. 1998; 24 (5):869–875. [PubMed: 9586819]
3. Bialik S, Geenen DL, Sasson IE, Cheng R, Horner JW, Evans SM, Lord EM, Koch CJ, Kitsis RN. Myocyte apoptosis during acute myocardial infarction in the mouse localizes to hypoxic regions but occurs independently of p53. J Clin Invest. 1997; 100 (6):1363. [PubMed: 9294101]
4. McGill CJ, Brooks G. Cell cycle control mechanisms and their role in cardiac growth. Cardiovasc Res. 1995; 30 (4):557–569. [PubMed: 8575004]

5. Rumyantsev PP. Interrelations of the proliferation and differentiation processes during cardiac myogenesis and regeneration. Int Rev Cytol. 1977; 51:187–273.
6. Kajstura J, Leri A, Finato N, Di Loreto C, Beltrami CA, Anversa P. Myocyte proliferation in end–stage cardiac failure in humans. Proc Natl Acad Sci USA. 1998; 95 (15):8801. [PubMed: 9671759]
7. Garg S, Narula J, Chandrashekhar Y. Apoptosis and heart failure: clinical relevance and therapeutic target. J Molec Cell Cardiol. 2005; 38 (1):73–79. [PubMed: 15623423]
8. Park M, Shen YT, Gaussin V, Heyndrickx GR, Bartunek J, Resuello RRG, Natividad FF, Kitsis RN, Vatner DE, Vatner SF. Apoptosis predominates in nonmyocytes in heart failure. Am J Physiol Heart Circ. 2009; 297 (2):H785.
9. Buja LM, Vela D. Cardiomyocyte death and renewal in the normal and diseased heart. Cardiovasc Pathol. 2008:1–26.10.1016/j.carpath.2008.02.004 [PubMed: 18160054]
10. Hockenbery DM, Oltvai ZN, Yin XM, Milliman CL, Korsmeyer SJ. Bcl-2 functions in an antioxidant pathway to prevent apoptosis. Cell. 1993; 75 (2):241–251. [PubMed: 7503812]
11. Maulik N, Engelman RM, Rousou JA, Flack JE III, Deaton D, Das DK. Ischemic preconditioning reduces apoptosis by upregulating anti-death gene Bcl-2. Circ. 1999; 100(90002):II-369.
12. Huang J, Ito Y, Morikawa M, Uchida H, Kobune M, Sasaki K, Abe T, Hamada H. Bcl-xL gene transfer protects the heart against ischemia/reperfusion injury. Biochem Biophys Res Commun. 2003; 311 (1):64–70. [PubMed: 14575695]
13. Potts MB. Reduced Apaf-1 levels in cardiomyocytes engage strict regulation of apoptosis by endogenous XIAP. J Cell Biol. 2005; 171(6):925–930.10.1083/jcb.200504082 [PubMed: 16344307]
14. Jolly S, Kane W, Bailie M, Abrams G, Lucchesi B. Canine myocardial reperfusion injury. Its reduction by the combined administration of superoxide dismutase and catalase. Circ Res. 1984; 54 (3):277. [PubMed: 6697450]
15. Khaper N, Kaur K, Li T, Farahmand F, Singal P. Antioxidant enzyme gene expression in congestive heart failure following mycardial infarction. Mol Cell Biochem. 2003; 251 (1):9–15. [PubMed: 14575298]
16. Andreka P, Zang J, Dougherty C, Slepak TI, Webster KA, Bishopric NH. Cytoprotection by Jun kinase during nitric oxide-induced cardiac myocyte apoptosis. Circ Res. 2001; 88 (3):305. [PubMed: 11179198]
17. Minamino T, Yujiri T, Papst PJ, Chan ED, Johnson GL, Terada N. MEKK1 suppresses oxidative stress-induced apoptosis of embryonic stem cell-derived cardiac myocytes. Proc Natl Acad Sci USA. 1999; 96 (26):15127. [PubMed: 10611349]
18. Franke TF, Kaplan DR, Cantley LC. PI3K: downstream AKTion blocks apoptosis. Cell. 1997; 88 (4):435. [PubMed: 9038334]
19. Wang Y, Huang S, Sah VP, Ross J, Brown JH, Han J, Chien KR. Cardiac muscle cell hypertrophy and apoptosis induced by distinct members of the p38 mitogen-activated protein kinase family. J Biol Chem. 1998; 273 (4):2161. [PubMed: 9442057]
20. Chen Z, Chua CC, Ho YS, Hamdy RC, Chua BHL. Overexpression of Bcl-2 attenuates apoptosis and protects against myocardial I/R injury in transgenic mice. Am J Physiol Heart Circ. 2001; 280 (5):H2313.
21. Chen Z, Siu B, Ho YS, Vincent R, Chua CC, Hamdy RC, Chua BHL. Overexpression of MnSOD protects against myocardial ischemia/reperfusion injury in transgenic mice. J Molec Cell Cardiol. 1998; 30 (11):2281–2289. [PubMed: 9925365]
22. Chua CC, Gao J, Ho YS, Xiong Y, Xu X, Chen Z, Hamdy RC, Chua BHL. Overexpression of IAP-2 attenuates apoptosis and protects against myocardial ischemia/reperfusion injury in transgenic mice. Biochim Biophys Acta Molec Cell Res. 2007; 1773 (4):577–583.
23. Matherne GP, Linden J, Byford AM, Gauthier NS, Headrick JP. Transgenic A1 adenosine receptor overexpression increases myocardial resistance to ischemia. Proc Natl Acad Sci USA. 1997; 94 (12):6541. [PubMed: 9177254]
24. Matsui T, Tao J, del Monte F, Lee KH, Li L, Picard M, Force TL, Franke TF, Hajjar RJ, Rosenzweig A. Akt activation preserves cardiac function and prevents injury after transient cardiac ischemia in vivo. Circ. 2001; 104 (3):330.

25. Harris JM, Chess RB. Effect of pegylation on pharmaceuticals. Nat Rev Drug Discov. 2003; 2 (3): 214–221. [PubMed: 12612647]
26. Hsieh PCH, Davis ME, Gannon J, MacGillivray C, Lee RT. Controlled delivery of PDGF-BB for myocardial protection using injectable self-assembling peptide nanofibers. J Clin Invest. 2006; 116 (1):237–248. [PubMed: 16357943]
27. Lee S, Murthy N. Targeted delivery of catalase and superoxide dismutase to macrophages using folate. Biochem Biophys Res Commun. 2007; 360 (1):275–279. [PubMed: 17586472]
28. Lee S, Yang SC, Heffernan MJ, Taylor WR, Murthy N. Polyketal microparticles: a new delivery vehicle for superoxide dismutase. Bioconj Chem. 2007; 18 (1):4–7.
29. Sy J, Phelps E, García A, Murthy N, Davis M. Surface functionalization of polyketal microparticles with nitrilotriacetic acid-nickel complexes for efficient protein capture and delivery. Biomater. 2010; 31 (18):4987–4994.
30. Sy J, Seshadri G, Yang S, Brown M, Oh T, Dikalov S, Murthy N, Davis M. Sustained release of a p38 inhibitor from non-inflammatory microspheres inhibits cardiac dysfunction. Nat Mater. 2008; 7 (11):863–868. [PubMed: 18931671]
31. Sutton MG, Sharpe N. Left ventricular remodeling after myocardial infarction: pathophysiology and therapy. Circ. 2000; 101 (25):2981.
32. Aso S, Ise H, Takahashi M, Kobayashi S, Morimoto H, Izawa A, Goto M, Ikeda U. Effective uptake of N-acetylglucosamine-conjugated liposomes by cardiomyocytes in vitro. J Control Release. 2007; 122 (2):189–198. [PubMed: 17681632]
33. Ise H, Kobayashi S, Goto M, Sato T, Kawakubo M, Takahashi M, Ikeda U, Akaike T. Vimentin and desmin possess GlcNAc-binding lectin-like properties on cell surfaces. Glycobiol. 2010; 20 (7):843.
34. Vemuri S, Rhodes C. Preparation and characterization of liposomes as therapeutic delivery systems: a review. Pharm Acta Helv. 1995; 70 (2):95–111. [PubMed: 7651973]
35. Seshadri G, Sy JC, Brown M, Dikalov S, Yang SC, Murthy N, Davis ME. The delivery of superoxide dismutase encapsulated in polyketal microparticles to rat myocardium and protection from myocardial ischemia-reperfusion injury. Biomater. 2010; 31 (6):1372–1379.
36. Yuan XB, Gu MQ, Kang CS, Zhao YH, Tian NJ, Pu PY, Sheng J. Surface biofunctionalization of PLA nanoparticles through amphiphilic polysaccharide coating and ligand coupling: Evaluation of biofunctionalization and drug releasing behavior. Carbohydr Polym. 2007; 67 (3):417–426.
37. Granger BL, Lazarides E. Desmin and vimentin coexist at the periphery of the myofibril Z disc. Cell. 1979; 18 (4):1053–1063. [PubMed: 391403]
38. Li Z, Mericskay M, Agbulut O, Butler-Browne G, Carlsson L, Thornell LE, Babinet C, Paulin D. Desmin is essential for the tensile strength and integrity of myofibrils but not for myogenic commitment, differentiation, and fusion of skeletal muscle. J Cell Biol. 1997; 139 (1):129–144. [PubMed: 9314534]
39. Bogoyevitch MA, Gillespie-Brown J, Ketterman AJ, Fuller SJ, Ben-Levy R, Ashworth A, Marshall CJ, Sugden PH. Stimulation of the stress-activated mitogen-activated protein kinase subfamilies in perfused heart. p38/RK mitogen-activated protein kinases and c-Jun N-terminal kinases are activated by ischemia/reperfusion. Circ Res. 1996; 79 (2):162–173. [PubMed: 8755992]
40. Pombo CM, Bonventre JV, Avruch J, Woodgett JR, Kyriakis JM, Force T. The stress-activated protein kinases are major c-Jun amino-terminal kinases activated by ischemia and reperfusion. J Biol Chem. 1994; 269 (42):26546–26551. [PubMed: 7929379]
41. Yin T, Sandhu G, Wolfgang CD, Burrier A, Webb RL, Rigel DF, Hai T, Whelan J. Tissue specific pattern of stress kinase activation in ischemia/reperfused heart and kidney. J Biol Chem. 1997; 272:19943–19950. [PubMed: 9242662]
42. Amado LC, Saliaris AP, Schuleri KH, St John M, Xie JS, Cattaneo S, Durand DJ, Fitton T, Kuang JQ, Stewart G, Lehrke S, Baumgartner WW, Martin BJ, Heldman AW, Hare JM. Cardiac repair with intramyocardial injection of allogeneic mesenchymal stem cells after myocardial infarction. Proc Natl Acad Sci USA. 2005; 102 (32):11474–11479. [PubMed: 16061805]
43. Krause K, Jaquet K, Schneider C, Haupt S, Lioznov MV, Otte KM, Kuck KH. Percutaneous intramyocardial stem cell injection in patients with acute myocardial infarction: first-in-man study. Heart. 2009; 95 (14):1145–1152. [PubMed: 19336430]

44. Herreros J, Prosper F, Perez A, Gavira JJ, Garcia-Velloso MJ, Barba J, Sanchez PL, Canizo C, Rabago G, Marti-Climent JM, Hernandez M, Lopez-Holgado N, Gonzalez-Santos JM, Martin-Luengo C, Alegria E. Autologous intramyocardial injection of cultured skeletal muscle-derived stem cells in patients with non-acute myocardial infarction. Eur Heart J. 2003; 24 (22):2012–2020. [PubMed: 14613737]

45. Li Q, Li B, Wang X, Leri A, Jana KP, Liu Y, Kajstura J, Baserga R, Anversa P. Overexpression of insulin-like growth factor-1 in mice protects from myocyte death after infarction, attenuating ventricular dilation, wall stress, and cardiac hypertrophy. J Clin Invest. 1997; 100 (8):1991–1999. [PubMed: 9329962]

46. Sabbah HN, Sharov VG, Gupta RC, Todor A, Singh V, Goldstein S. Chronic therapy with metoprolol attenuates cardiomyocyte apoptosis in dogs with heart failure. J Am Coll Cardiol. 2000; 36 (5):1698–1705. [PubMed: 11079679]

47. Jones SP, Zachara NE, Ngoh GA, Hill BG, Teshima Y, Bhatnagar A, Hart GW, Marban E. Cardioprotection by N-acetylglucosamine linkage to cellular proteins. Circulation. 2008; 117 (9): 1172. [PubMed: 18285568]

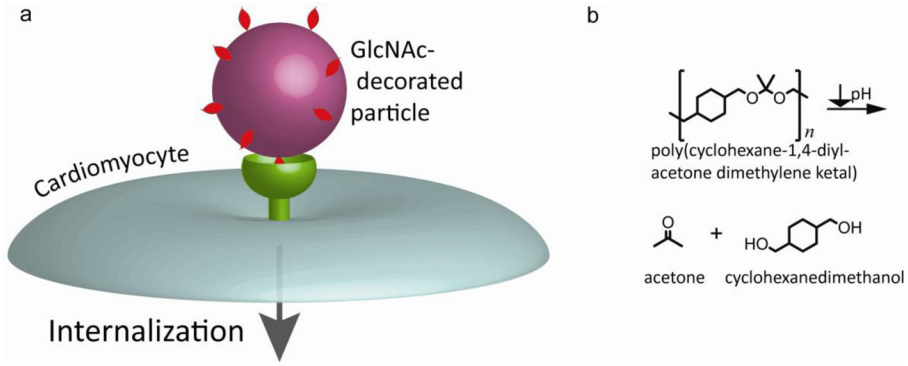

Figure 1. Overall scheme for proposed GlcNAc-mediated drug delivery system

(a) Decoration of drug-loaded polymeric nanoparticle with GlcNAc should provide a mechanism whereby therapeutics may be delivered intracellularly to CMs. (b) The particle will be composed of the acid-labile poly(cyclohexane-1,4-diyl acetone dimethylene ketal) (PCADK). Once internalized, the particle will degrade into the biocompatible products acetone and cyclohexanedimethanol.

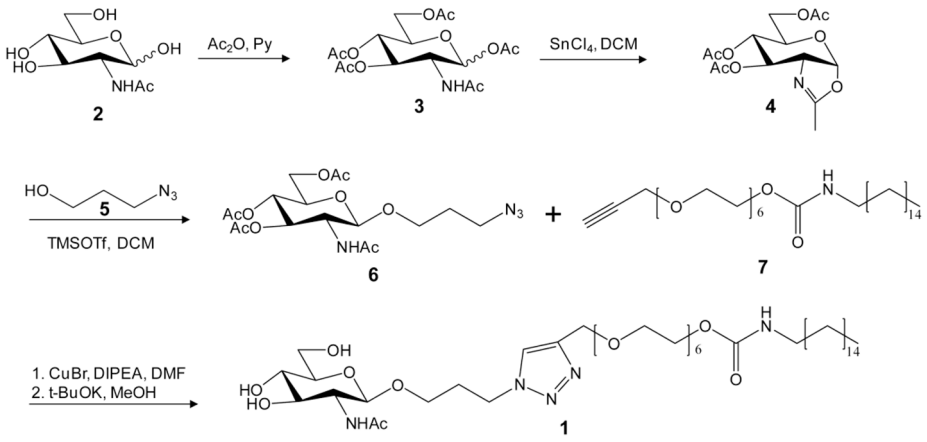

Figure 2. Synthesis of GlcNAc-alkyl

A facile and scalable 8-step process is followed to produce the tethering and targeting compound GlcNAc-alkyl. During nanoparticle production, the hydrophobic alkyl chain associates with the polymeric particle and the hydrophilic carbohydrate headgroup is free to interact with CMs.

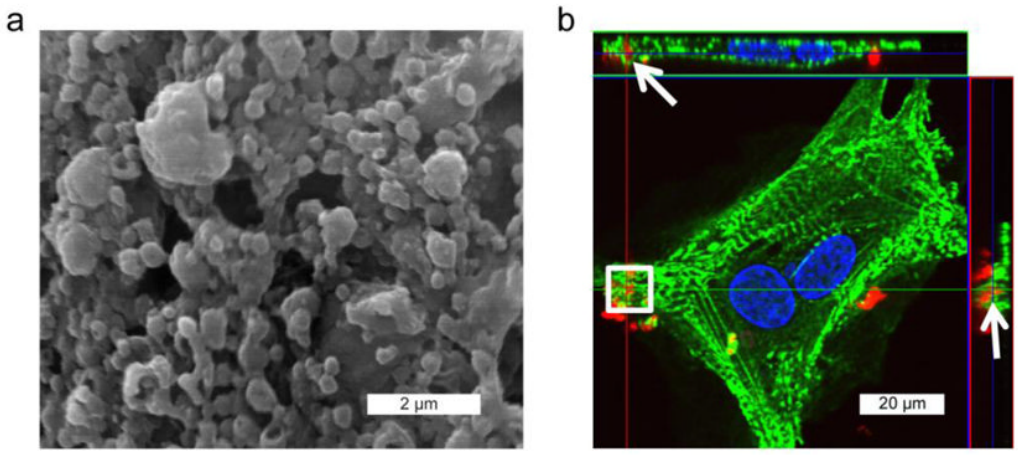

Figure 3. Incubation of CMs with PK-GlcNAc-rhodamine particles for internalization verification

(a) Rhodamine-loaded particles (diameter=320±156 nm) were decorated with GlcNac-alkyl and imaged by SEM. (b) Cultured CMs were treated with PK-GlcNAc-rhodamine particles for 12h before fixation in paraformaldehyde and immunostaining for CM-specific α-actinin (green) and DAPI for nuclei (blue). Confocal microscopy afforded orthogonal views of the cell, by which internalized nanoparticles (red) can be observed in the same plane as the α-actinin (arrows).

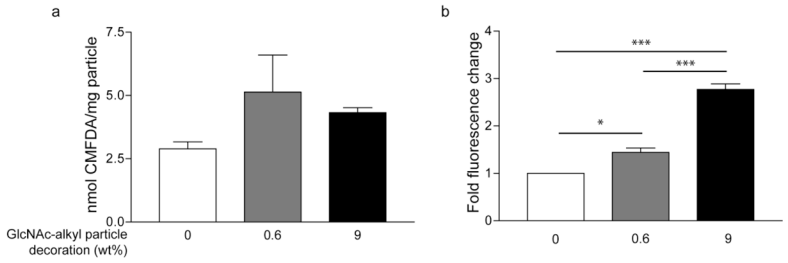

Figure 4. Measurement of particle internalization by CMFDA fluorescence demonstrating increased uptake

PK-GlcNAc-CMFDA nanoparticles were decorated with 0%, 0.6%, or 9% GlcNAc-alkyl by weight and loaded with the cell tracker dye, 5-chloromethylfluorescein diacetate (CMFDA). (a) Particles are closely load-matched for CMFDA content: 0%, 0.6% and 9% decorated particles contained 2.9±0.3, 5.1±1.5, and 4.3±0.2 nmol CMFDA/mg particle, respectively. Data are expressed as mean±SEM from three experiments. (b) After incubation of CMs with particles, fluorescence of cell culture was obtained by plate reader and normalized to 0% GlcNAc-alkyl decoration and respective particle CMFDA content. The positive correlation between fluorescence and degree of decoration indicates a dose response and confirms cell uptake of GlcNAc-decorated particles. Data are expressed as mean±SEM from four separate experiments (*p<0.05, ***p<0.001; ANOVA followed by Newman-Keuls post-test).

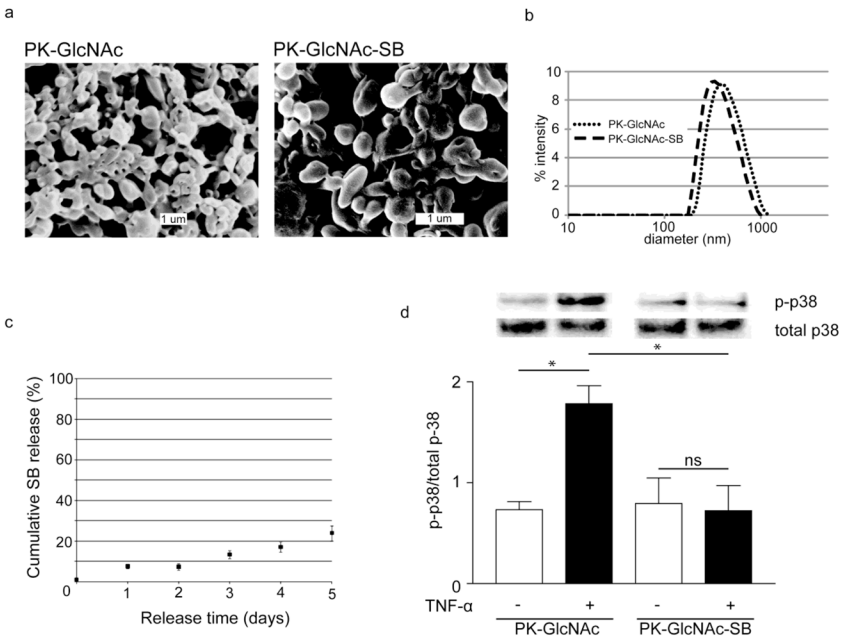

Figure 5. Treatment of CMs *in vitro* with p38 inhibitor-loaded nanoparticles reduces TNF-α stimulated p38 activation

PK-GlcNAc and PK-GlcNAc-SB particles were imaged via (a) SEM (diameter=407±125 nm or d=342±165 nm, respectively) and (b) analyzed by DLS (diameter=465±173 nm or diameter=395±145 nm, respectively). Data are mean±SD. (c) PK-GlcNAc-SB particles release cargo through diffusion at pH 7.4. (d) PK-GlcNAc did not prevent p38 phosphorylation, as demonstrated by a 2.4-fold increase of p-p38 due to TNF-α treatment. However, PK-GlcNAc-SB treatment significantly inhibited p38 activation compared with empty particles. Data are mean±SEM and are expressed as a ratio of phosphorylated to total p38 (n=3; *p<0.05; ANOVA followed by Tukey post-test.)

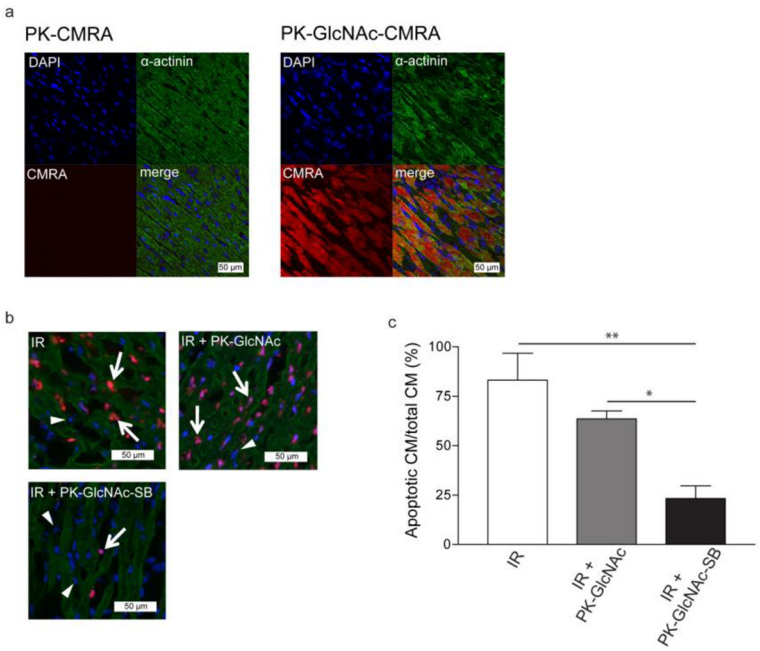

Figure 6. GlcNAc decoration enhances particle uptake *in vivo* following IR and reduces apoptotic events

(a) Rats that received myocardial injection of (9′-(4-(and 5)-chloromethyl-2-carboxyphenyl)-7′-chloro-6′-oxo-1,2,2,4-tetramethyl-1,2-dihydropyrido[2′,3′-6]xanthene (CMRA)-loaded GlcNAc-decorated particles (PK-GlcNAc-CMRA) immediately following IR exhibited a greater CMRA fluorescence three days post-IR than animals that had received PK-CMRA particles, indicating enhanced *in vivo* uptake due to GlcNAc decoration. (b and c) Immediately following IR, particles were injected intramyocardially and hearts removed one day post-IR. TUNEL staining indicated apoptotic nuclei (b) (apoptotic nuclei [purple] indicated by arrow, non-apoptotic nuclui [blue] indicated by triangle), and comparison against total cardiomyocyte nuclei indicated that animals that received PK-GlcNAc-SB particle injections achieved 3.6-fold fewer apoptotic events in the injured myocardium compared to IR and 2.7-fold fewer than the PK-GlcNAc group (c). (n=3 for each group). Data are mean±SEM. *p<0.05, *p<0.01. ANOVA followed by Newman-Keuls post-test.

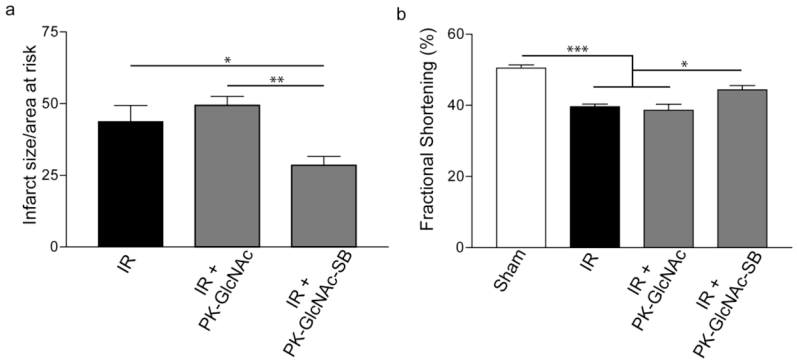

Figure 7. Infarct size reduction and functional improvements seen in PK-GlcNAc-SB treatment following ischemia-reperfusion injury

Immediately following IR, particles were injected directly into the injured myocardium. Three days following surgery, echocardiography was performed and heart cross sections analyzed for infarct size. (a) The ratio of infarct size to area at risk was calculated for the treatment groups. PK-GlcNAc treatment had no significant effect, but PK-GlcNAc-SB treatment significantly decreased infarct size compared to both treatment groups (mean ±SEM, n=5; *p<0.05, **p<0.01; ANOVA followed by Newman-Keul multiple comparison post-test). (b) Fractional shortening calculated from echocardiographic measurements demonstrated a significant decrease in function in IR animals compared to sham. There was no significant improvement seen with PK-GlcNAc, though PK-GlcNAc-SB treatment improved function compared with other IR groups. (n=4 for sham n>7 for IR groups). Data are mean±SEM. *p<0.05, ***p<0.001. ANOVA followed by Tukey post-test.